4th International Conference on Jets, Wakes and Separated Flows, ICJWSF2013
September 17-21, 2013, Nagoya, JAPAN

STIRRING AND MIXING BY GRID-GENERATED TURBULENCE IN THE PRESENCE OF A MEAN SCALAR GRADIENT

*[1]S. Laizet & *[1]J.C. Vassilicos

*[1]Department of Aeronautics, Imperial College London
South Kensington Campus, London, UK
s.laizet@imperial.ac.uk
j.c.vassilicos@imperial.ac.uk

ABSTRACT

The stirring and mixing of a passive scalar by grid-generated turbulence in the presence of a mean scalar gradient is studied in three dimensions by DNS (Direct Numerical Simulation). Using top-end high fidelity computer simulations, we calculate and compare the effects of various fractal and regular grids on scalar transfer and turbulent diffusion efficiencies. We demonstrate the existence of a new mechanism present in turbulent flows generated by multiscale/fractal objects and which has its origin in the multiscale/fractal space-scale structure of such turbulent flow generators. As a result of this space-scale unfolding (SSU) mechanism, fractal grids can enhance scalar transfer and turbulent diffusion by one order of magnitude while at the same time reduce pressure drop by half. The presence of this SSU mechanism when turbulence is generated by fractal grids means that the spatial distribution of length-scales unfolds onto the streamwise extent of the flow and gives rise to a variety of wake-meeting distances downstream. This SSU mechanism must be playing a decisive role in environmental, atmospheric, ocean and river transport processes wherever turbulence originates from multiscale/fractal objects such as trees, forests, mountains, rocky river beds and coral reefs. It also ushers in the new concept of fractal design of turbulence which may hold the power of setting entirely new mixing and cooling industrial standards.

1. INTRODUCTION

Recently, [4, 8, 9, 10, 17, 3] used different multiscale grids to generate turbulence in a wind tunnel or in a water tank and have shown that complex multiscale boundary/initial conditions can drastically influence the behaviour of a turbulent flow, especially when a fractal square grid (see figure 1) is placed at the entry of a wind tunnel test section. Fractal geometry is a concept where a given pattern is repeated and split into parts, each being a reduced-copy of the whole. Multiscale (fractal) objects can be designed to be immersed in any fluid flow where there is a need to control and design the turbulence generated by the object. The experiments have shown that, unlike regular objects (where the turbulence is generated by only one scale), a slight modification of one of the multiscale object's parameters can deeply modify the turbulence generated by the fluid's impact on the object. Multiscale objects offer the opportunity to discover new complex flow effects/interactions that can help understand how to control and/or manage complex fluid flows. Furthermore, such multiscale objects can be designed as energy-efficient mixers with high turbulent intensities and a small pressure drop [7]. [1] have also shown experimentally that fractal grids can be designed as stirring elements for inline static mixers and, as such, that they compare favourably with commercially available state-of-the-art stirring elements.

In this computational study we calculate and compare the effects of various fractal and regular grids on scalar transfer and turbulent diffusion efficiencies [13, 18, 16]. As a result we report on a new mechanism which greatly increases scalar transfer and turbulent diffusion and at the same time reduces pressure drop and therefore power losses.

The organisation of this paper is as follows. In the following section, we present the DNS methodology, a brief description of the grids and the numerical parameters of each simulation. Some results about the turbulence and the flow field downstream of the grid are discussed in the following section. Then, passive scalar results are presented, followed by a conclusion.

2. FLOW PARAMETERS AND NUMERICAL MODELLING

2.1 Numerical Methods

To solve the incompressible Navier-Stokes equations and the transport equation for the passive scalar, we use a numerical code (called **Incompact3d**) based on sixth-order compact schemes for spatial discretization and a third order Adams-Bashforth scheme for time advancement. To treat the incompressibility condition, a fractional step method requires to solve a Poisson equation. This equation is fully solved in spectral space, via the use of relevant 3D Fast Fourier Transforms. The pres-

	$n_x \times n_y \times n_z$	$L_x \times L_y \times L_z$ (t_{min})	Grid	It.	κ	S t_{min}	σ	M_{eff}
DNS1	2305×288×288	768×96×96	□	3	10ν	1/16	0.3	$14.7t_{min}$
DNS2	2305×288×288	768×96×96	I	3	10ν	1/16	0.3	$23.4t_{min}$
DNS3	2881×360×360	1152×144×144	□	4	10ν	1/16	0.5	$6.5t_{min}$
DNS4	2881×180×180	1152×72×72	Reg.		10ν	1/16	0.5	$6.5t_{min}$

Table 1 Numerical parameters of the simulations and characteristics of the grids.

sure mesh is staggered from the velocity mesh by half a mesh, to avoid spurious pressure oscillations. With the help of the concept of modified wave number, the divergence free condition is ensured up to machine accuracy. More details about the present code and its validations, especially the original treatment of the pressure in the spectral space, can be found in [5]. The modelling of the grids is performed by an Immersed Boundary Method, following a procedure proposed by [11]. The present method is a direct forcing approach that ensures the no-slip boundary condition at the grid walls. It mimics the effects of a solid surface on the fluid with an extra forcing in the Navier-Stokes equations.

Because of the size of the simulations, the parallel version of **Incompact3d** has been used for this numerical work. Based on a highly scalable 2D decomposition library and a distributed FFT interface, it is possible to use the code on thousands of computational cores. More details about this efficient parallel strategy can be found in [6].

2.2 Governing equations

The governing equations for the incompressible velocity field are the forced Navier-Stokes equations:

$$\frac{\partial \mathbf{u}}{\partial t} = -\nabla p - \frac{1}{2}\left[\nabla\left(\mathbf{u}\otimes\mathbf{u}\right) + \left(\mathbf{u}.\nabla\right)\mathbf{u}\right] + \nu\nabla^2\mathbf{u} + \mathbf{f} \quad (1)$$

$$\nabla.\mathbf{u} = \mathbf{0} \quad (2)$$

where $p(\mathbf{x},\mathbf{t})$ is the pressure field (for a fluid with a constant density $\rho = 1$) and $\mathbf{u}$ the velocity field. The forcing field $\mathbf{f}(\mathbf{x},\mathbf{t})$ is used through an Immersed Boundary Method in order to take into account the grid inside the computational domain. $\mathbf{x} \equiv (x, y, z)$ are the spatial coordinates in the streamwise (x) and two spanwise directions.

The scalar field $\theta(\mathbf{x},\mathbf{t})$ is advected by the velocity field and diffused by molecular processes, i.e. our code solves

$$\frac{\partial \theta}{\partial t} + \mathbf{u}\cdot\nabla\theta = \kappa\nabla^2\theta \quad (3)$$

with molecular diffusivity $\kappa = 10\nu$. The initial condition we impose on this scalar field is $\theta(\mathbf{x},\mathbf{0}) = \mathbf{Sy}$ where S is a constant scalar gradient and the inflow condition is $\theta = Sy$ at all time. The other boundary conditions for θ are outflow in the streamwise end of the computational domain, periodic in the z direction and Neumann in the y direction. These conditions are the simplest way to initiate and sustain a turbulent scalar flux [2, 19, 18]

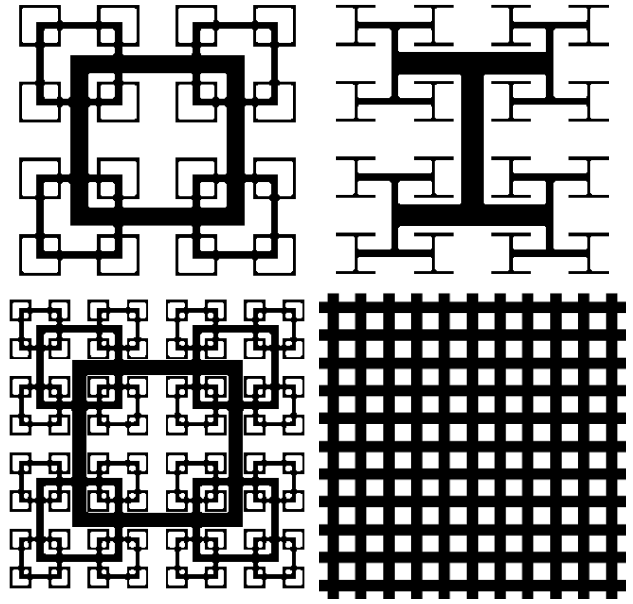

Fig. 1 Scaled diagrams of the four grids used in this study. From left to right: fractal square grid with 3 fractal iterations, I grid with 3 fractal iterations, square grid with 4 fractal iterations and regular grid.

2.3 Numerical Parameters

As shown in Figure 1, four different grids are used in this numerical work to investigate the streamwise evolution of the stirring and mixing of a passive scalar in the presence of a mean scalar gradient. We considered two families of fractal grids each based on a different fractal-generating pattern [4]. The two patterns can be distinguished by the number of rectangular bars they require, 3 for the I grid and 4 for the square grids. These fractal grids are completely characterised by the choice of the pattern and:

- the number of fractal iterations N, here $N = 3$ for the fractal I grid and $N = 3, 4$ for the fractal square grids,
- the bars' lengths $L_j = R_L^j L_0$ and lateral thicknesses $t_j = R_t^j t_0$ (in the plane of the grid, normal to the mean flow) at iteration j, $j = 0, ..., N-1$. Here, $R_L = 1/2$, $L_0 = 0.5L_y$ for all the fractal grids, where L_y and L_z (with $L_y = L_z$) are the lateral sizes of the computational domain. By definition, $L_0 = L_{max}$, $L_{N-1} = L_{min}$, $t_0 = t_{max}$ and $t_{N-1} = t_{min}$. Note that, in the present work, t_{min} is set to

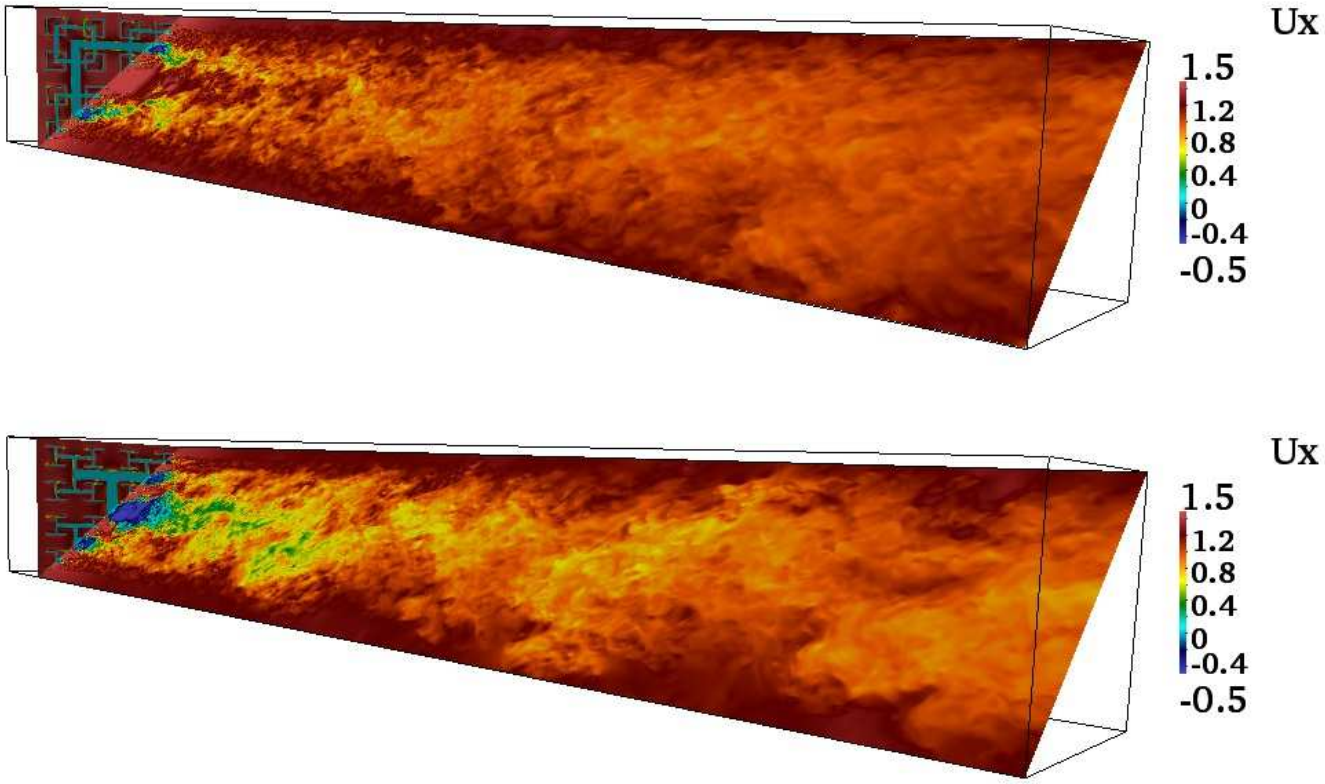

Fig. 2 Instantaneous streamwise velocity field obtained for the fractal grid with three fractal iterations: DNS1 with square pattern (top) and DNS 2 with I pattern (bottom)

the same value for all fractal grids,

- the number 4^j of patterns at iteration j
- the thickness ratio $t_r \equiv t_{max}/t_{min}$, i.e. the ratio between the lateral thickness of the bars making the largest pattern and the lateral thickness of the smallest. $t_r = 8.67$ for the fractal square grid with three iterations, $t_r = 10.5$ for the fractal I grid and $t_r = 8.5$ for the fractal square grid with four fractal iterations.

The blockage ratio σ of our fractal grids defined as the ratio of their total area in the lateral plane to the area $T^2 = L_y \times L_z$, are determined by our choices of the previous parameters and are given in Table 1.

Unlike regular grids, multiscale/fractal grids do not have a well-defined mesh size. This is why [4] introduced an effective mesh size for multiscale grids, $M_{eff} = \frac{4T^2}{L_G}\sqrt{1-\sigma}$ where L_G is the perimeter length in the $(y-z)$ plane of the fractal grid. The multiscale nature of multiscale/fractal grids influences M_{eff} via the perimeter P which can be extremely long in spite of being constrained to fit within the area $T^2 = L_y \times L_z$. However, this definition of M_{eff} also returns the regular mesh size M, when applied to our regular grid. The effective mesh size is fully determined by our choices of parameters characterising the fractal grids and is given in Table 1. The regular grid considered here has the same blockage ratio as the fractal square grid with four iterations. The lateral thickness b of this regular grid is $2.6t_{min}$. Note finally that the streamwise thickness of the bars is $3.2t_{min}$ for the four grids used in this numerical study.

The computational domain and number of mesh nodes for each simulation are given in Table 1. For the velocity field, inflow/outflow boundary conditions are used in the x-direction and periodic boundary conditions in the y direction for $-L_y/2$ and $L_y/2$ and in the z direction $-L_z/2$ and $L_z/2$. For each grid, the simulation is performed with a Reynolds number $Re_{t_{min}} = 300$ (based on the smallest lateral thickness t_{min} of the fractal grids and the streamwise upstream velocity U_∞).

3. FLOW FIELD AND TURBULENCE

Figures 2 and 3 illustrate the turbulent flows obtained from the four DNS by showing snapshots of instantaneous streamwise velocity fields for a diagonal plane. A non-homogeneous turbulent field is obtained close to the grids, but in the case of the regular grid (DNS4), the turbulence does homogenise relatively close to the grid. Instead, the turbulence remains non-homogeneous for a long distance downstream of the fractal grids (DNS1, DNS2 and DNS3). There is a clear

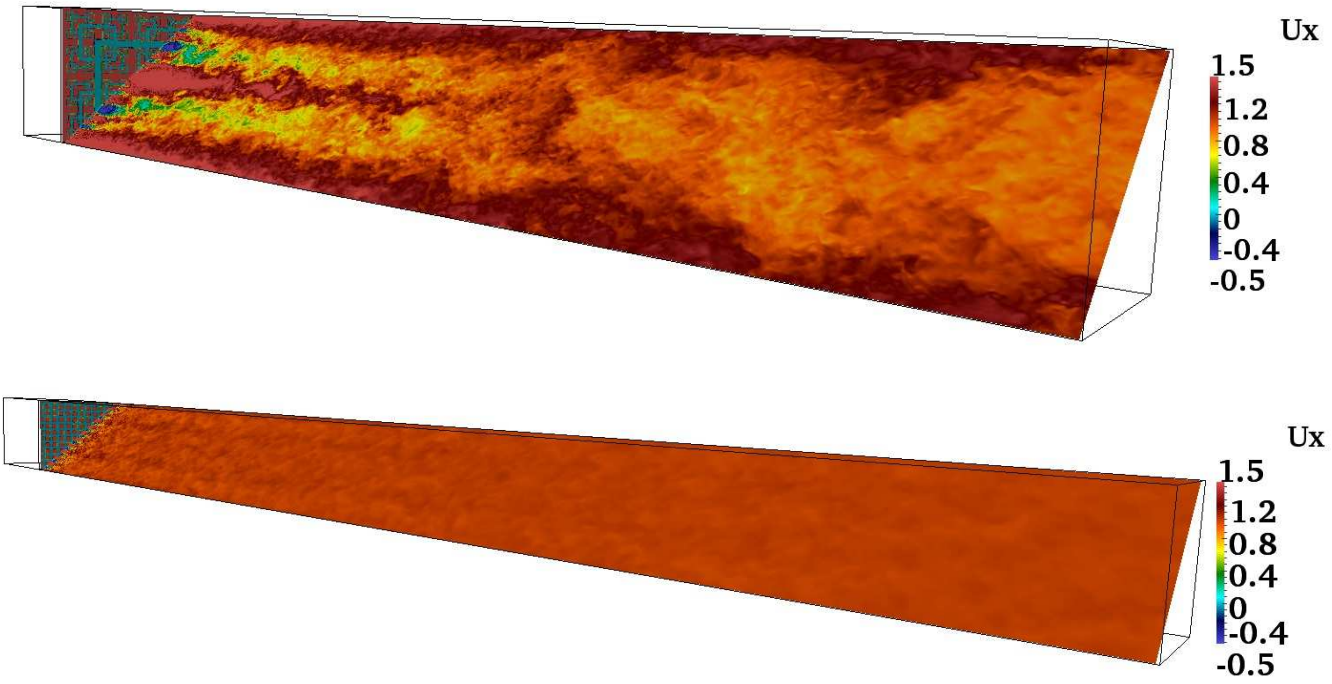

Fig. 3 Instantaneous streamwise velocity field obtained for DNS3 with the fractal square grid with four fractal iterations (top) and for DNS4 with a regular grid (bottom).

presence of wakes of different sizes, corresponding to the fractal iterations of the grids. These snapshots suggest that the levels of turbulence generated by the fractal grids seem to be more intense than for a regular grid, except very close to the grid. It can also be seen that the I grid with three fractal iterations is generating more turbulence than the square grid with three fractal iterations, even if they have the same blockage ratio. We can therefore expect to have strong different behaviours for our passive scalar fields depending on the turbulent generator.

Figure 4 shows the streamwise evolution of $< u'^2 >^{0.5} /U_\infty$ and $< p > /0.5\rho U_\infty^2$ (where p is the pressure divided by the fluid's mass density) for the four different grids with respect to x/M_{eff}. The regular grid generates a much higher peak average turbulence (more than 55%) than the three fractal grids. However, the average turbulence decay is much slower for the fractal grids whereas a very fast decrease can be observed for the regular grid. It should be noted that the spatial location of the peak of turbulence is approximately at a distance of $1M_{eff}$ from the grid. At a distance of $35M_{eff}$ from the grid, the average turbulence for the fractal square grid with four fractal iterations is about 15% whereas for the regular grid it is only about 2.5% (same blockage ratio for the two grids). Another important result is the confirmation [4] that for the grids with three fractal iterations with a similar blockage ratio, the I grid generates more turbulence than the square grid, with a slower decay rate for the average turbulence.

The streamwise evolution of the pressure is consistent with the streamwise evolution of the average turbulence. For the regular grid the pressure drop is very important very close to the peak and then it remains constant at a low value whereas the three fractal square grids return a smaller pressure drop with a much longer pressure recovery length, especially for the grid with four fractal iterations (DNS3). As expected, DNS3 and DNS4 return a higher pressure drop than DNS1 and DNS2 (corresponding to the fractal grids with three fractal iterations) as their blockage ratio of 0.5 is higher than the one of 0.3 for DNS1 and DNS2. However, The pressure drop between upstream and far downstream in DNS3 is about half that in DNS4 even though the blockage ratio is the same. DNS1 and DNS2 have a similar low pressure drop even if the patterns of the grids are different.

4. PASSIVE SCALAR

One of the interesting results about the passive scalar is presented in Figure 5 (top) where we can observe a continuous increase for the passive scalar variance, much more pronounced for the fractal grids. For instance, at the end of the computational domain, the variance is more than ten times bigger for the fractal grid with four fractal iterations (DNS3) than for the regular grid (DNS4). One can assume that this is due to the scalar fluctuation S' which has been greatly enhanced by the

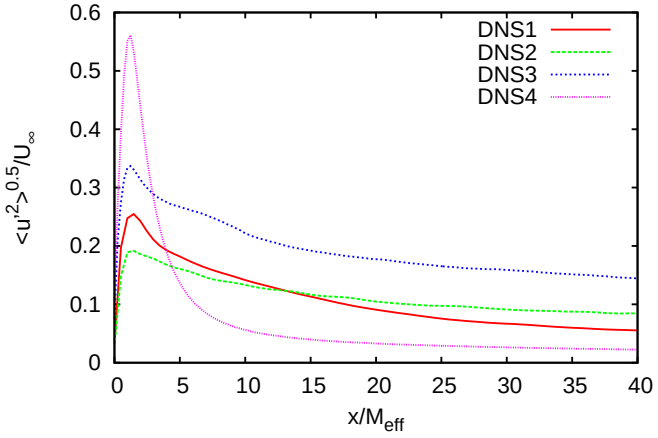

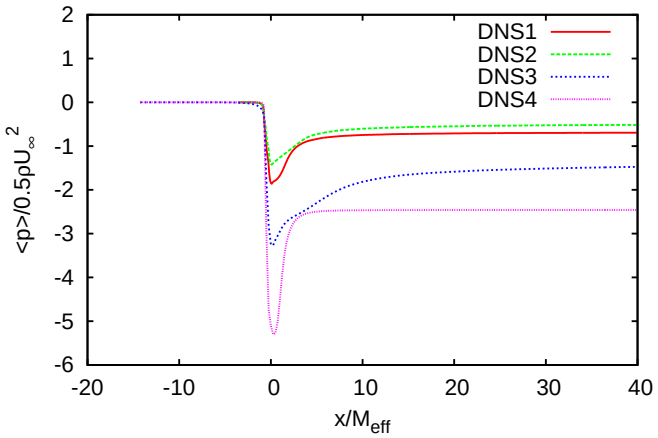

Fig. 4 Streamwise evolution of $< u'^2 >^{0.5} /U_\infty$ (top) and $< p > /0.5\rho U_\infty^2$ (bottom) where $< . >$ denotes an average in y and z over the collection time T.

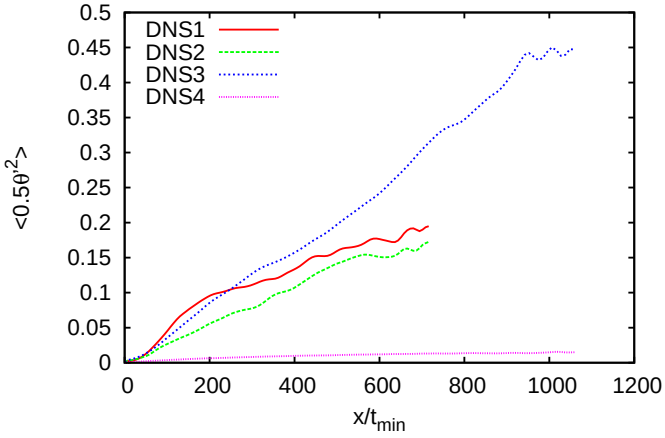

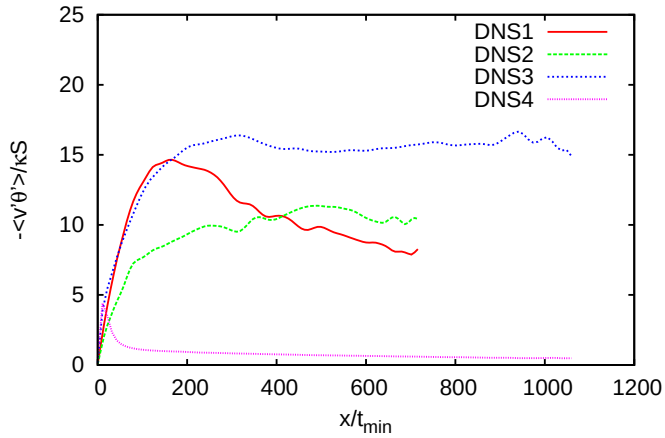

Fig. 5 Streamwise evolution of the variance $\frac{1}{2} < \theta'^2 >$ (left) and of $< v'\theta' > \kappa S$ (right). Data extracted for the four different grids corresponding to DNS1, DNS6, DNS9 and DNS10.

fractal-generated turbulence and is much stronger that the passive scalar dissipation. Furthermore, we notice a monotonic increase of the passive scalar variance for the four grids, in agreement with the experiments of [15, 14] where the authors found that the variance should grow linearly with streamwise distance in decaying turbulent grid flow. Finally, it should be noted that the rate of increase is different for different grids.

The streamwise evolution of the normalised transverse turbulent scalar transfer $< v'\theta' > /\kappa S$ for the four different grids is plotted in Figure 5 (bottom). Different behaviours can again be observed: for the regular grid (DNS4), the normalised transverse turbulent scalar transfer peaks very close to the grid and then decay very quickly. For the fractal square grid with four fractal iterations (DNS3) and for the fractal I grid (DNS2), the normalised transverse turbulent scalar transfer peaks at a further distance from the grid, just before $200t_{min}$ and then remain approximately constant until the end of the computational domain with a value of 16 for DNS3 and around 10 for DNS2. Finally, for the fractal square grid with three fractal iterations (DNS1), the normalised transverse turbulent scalar transfer also peaks just before $200t_{min}$ but then decay linearly from a value of about 15 to a value of about 7 at the end of the computational domain. The ratio of $< \theta' v' >$ for the fractal grid with four fractal iteration (DNS3) to $< \theta' v' >$ for the regular grid (DNS4) is oscillating between 19 at $x = 200t_{min}$ and 32 at the end of our computational domain.

5. CONCLUSION

Four spatially evolving turbulent flows generated by three fractal grids and a regular grid have been investigated by means of Direct Numerical Simulation. In this numerical work, we have focused on the stirring and mixing of a passive scalar in the presence of a mean scalar gradient. Different behaviours for different grids have been observed for the passive scalar variance and passive scalar flux. Those differences can be explained with the the space-scale unfolding (SSU) mechanism, introduced by [7].

The presence of the SSU mechanism when turbulence is generated by fractal grids means that, for the same blockage ratio, the spatial distribution of length-scales on the fractal grid unfolds onto the streamwise extent of the flow and gives rise to a variety of wake-

meeting distances downstream. As a result, the grids turbulence generation is distributed in the streamwise direction causing the turbulence to be less and the pressure drop smaller very near the grid by comparison to a same blockage regular grid, but a much longer pressure recovery and a much slower turbulence decay in multiples of M_{eff}.

This mechanism is absent from regular grid turbulence where all wakes meet their neighboring wakes at the same short distance from the grid causing a great burst of intense turbulence very near the grid and a fast decay of this turbulence. The SSU mechanism is also responsible for the great scalar transfer enhancement caused by the fractal grids, by an increase of the turbulent diffusivity and thereby scalar transfer.

Further simulations will be required to investigate in more detail the SSU mechanism. In particular, it could be interesting to tune S with respect to the dissipation so that we can study the passive scalar variance decrease in the streamwise direction. We will then be able to make comparisons with previous works [12, 14] where the properties of a passive scalar field with decaying variance were studied. Another future direction of investigation concerns the influence of the Prandtl number.

Acknowledgements

The authors are grateful to Dr. Ning Li for helping with the parallel version of **Incompact3d**. We also thank Eric Lamballais for very useful discussions and acknowledge support from EPSRC Research grants EP/E00847X/1 and EP/F051468/1.

REFERENCES

[1] C.J. Coffey, G.R. Hunt, R.E. Seoud, and J. C. Vassilicos. Mixing effectiveness of fractal grids for inline static mixers. In *Proof of Concept report for the attention of Imperial Innovations.*, http://www3.imperial.ac.uk/tmfc/papers/poc, 2007.

[2] S. Corrsin. Heat transfer in isotropic turbulence. *J. Applied Phys.*, **33(1)**:113–118, 1952.

[3] R. Gomes-Fernandes, B. Ganapathisubramani, and J. C. Vassilicos. PIV study of fractal-generated turbulence. *J. Fluid Mech.*, **701**:306–336, 2012.

[4] D. Hurst and J. C. Vassilicos. Scalings and decay of fractal-generated turbulence. *Phys. Fluids*, **19**(035103), 2007.

[5] S. Laizet and E. Lamballais. High-order compact schemes for incompressible flows: a simple and efficient method with the quasi-spectral accuracy. *J. Comp. Phys.*, **228(16)**:5989–6015, 2009.

[6] S. Laizet and N. Li. Incompact3d, a powerful tool to tackle turbulence problems with up to $o(10^5)$ computational cores. *Int. J. Numer. Methods Fluids*, **67(11)**:1735–1757, 2011.

[7] S. Laizet and J. C. Vassilicos. The fractal space-scale unfolding mechanism for energy-efficient turbulent mixing. *"Phys. Rev. E"*, **86(4)**:046302, 2012.

[8] N. Mazellier and J. C. Vassilicos. Turbulence without Richardson-Kolmogorov cascade. *Phys. Fluids*, **22**(075101), 2010.

[9] K. Nagata, H. Suzuki, H. Sakai, Y. Hayase, and T. Kubo. Direct numerical simulation of turbulent mixing in grid-generated turbulence. *Inter. Review of PHYSICS*, **132**:014054, 2008.

[10] F. Nicolleau, S. Salim, and A.F. Nowakowski. Experimental study of a turbulent pipe flow through a fractal plate. *J. Turbulence*, **12**:637046, 2011.

[11] P. Parnaudeau, J. Carlier, D. Heitz, and E. Lamballais. Experimental and numerical studies of the flow over a circular cylinder at Reynolds number 3 900. *Phys. Fluids*, **20**:085101, 2008.

[12] A. Pumir. A numerical study of the mixing of a passive scalar in three dimensions in the presence of a mean gradient. *Phys. Fluids*, **6**:2118, 1994.

[13] B.I. Shraiman and E.D. Siggia. Scalar turbulence. *Nature*, **6787**:639–646, 2000.

[14] A. Sirivat and Z. Warhaft. The effect of a passive cross-stream temperature gradient on the evolution of temperature variance and heat flux in grid turbulence. *J. Fluid Mech.*, **128**:323–346, 1983.

[15] P.J. Sullivan. Dispersion of a line source in grid turbulence. *Phys. Fluids*, **19**:159, 1976.

[16] H. Suzuki, K. Nagata, H. Sakai, and R. Ukai. High-schmidt-number scalar transfer in regular and fractal grid turbulence. *Phys. Scr.*, **T142**:014069, 2010.

[17] P. Valente and J. C. Vassilicos. The decay of turbulence generated by a class of multi-scale grids. *J. Fluid Mech.*, **687**:300–340, 2011.

[18] Z. Warhaft. Passive scalars in turbulent flows. *Ann. Rev. Fluid Mech.*, **32**:203–240, 2000.

[19] H.K. Wiskind. A uniform gradient turbulent transport experiment. *J. Geophysical Research*, **67**:30–33, 1962.